

Neutron emission in the reaction $^{165}\text{Ho} + ^{56}\text{Fe}$ at $E_{\text{lab}} = 8.5 \text{ MeV/u}$

D. Hilscher,* J. R. Birkelund, A. D. Hoover, W. U. Schröder, W. W. Wilcke, and J. R. Huizenga
Departments of Chemistry and Physics, University of Rochester, Rochester, New York 14627

A. C. Mignerey and K. L. Wolf
Argonne National Laboratory, Argonne, Illinois 60439

H. F. Breuer and V. E. Viola, Jr.
Department of Chemistry, University of Maryland, College Park, Maryland 20742
 (Received 8 March 1979)

Neutron emission and α -particle emission in the $^{165}\text{Ho} + ^{56}\text{Fe}$ reaction have been measured for the damped-collision and fusion-fission components of this reaction at a bombarding energy of 8.5 MeV/u. The c.m. neutron energy spectra for damped collisions indicate equal temperatures for the light and heavy fragments, a result consistent with the equilibration of the excitation energy during the interaction time. Pre-equilibrium neutron emission is found to contribute less than 5%. An out-of-plane neutron anisotropy $A_2 = 0.2 \pm 0.1$ is found. The measured ratios of the neutron multiplicities for the light and heavy fragments suggest a rapid approach of the fragment N/Z ratios during the collision to that corresponding to minimum potential energy of the composite system.

NUCLEAR REACTIONS $^{165}\text{Ho}(^{56}\text{Fe}, \text{HI}xn)E_{\text{lab}} = 476 \text{ MeV}$; measured $\sigma_n(E_n, \theta_n, \phi_n)$; deduced nuclear temperatures, neutron multiplicities, neutron-to-proton ratio N/Z , neutron out-of-plane anisotropy A_2 .

I. INTRODUCTION

The extensive study of heavy-ion reactions at a few MeV/u above the Coulomb barrier has led to important advances in understanding these reactions.¹ The experimental results suggest that a large fraction of the kinetic energy available in the entrance channel is converted within the short interaction time of 10^{-22} to 10^{-21} s into intrinsic excitation and collective rotational and deformation energy of the fragments. After the breakup of the intermediate complex into two final fragments the communication between the ions is terminated, and the excitation energy acquired by the two fragments leads to the evaporation of light particles such as neutrons, protons, and α particles, as well as γ -ray emission during the final stages of the de-excitation cascade.

Although emitted only in a secondary process, de-excitation particles from the final fragments carry important information on the damped-reaction mechanism, in particular on the energy-dissipation processes involved. Of considerable interest in this respect is the key question of the present investigation: whether or not statistical equilibration of the excitation-energy degree of freedom is achieved during the short interaction time encountered in a damped collision. Only if such an equilibration has occurred does one expect the final fragments to acquire the same nuclear temperature. Since the particle-evaporation

spectra reflect the fragment nuclear temperature, it is possible to investigate the energy-equilibration processes pertaining to damped collisions by measuring the secondary particles. The study of neutron emission is advantageous because of the absence of Coulomb effects which complicate the interpretation of charged-particle spectra in terms of a uniform nuclear temperature. A test of the degree of excitation-energy equilibration achieved in a damped collision is expected to be more conclusive for a system where the projectile (A_P) and target (A_T) masses are significantly different, since the reaction fragments from a symmetric system are more likely to exhibit similar excitation energies and temperatures in the exit channel. As a compromise between large projectile-target asymmetry and low fissility of the targetlike fragment, the system $^{165}\text{Ho} + ^{56}\text{Fe}$ with $A_T/A_P = 2.95$ was chosen in this work.

In addition to the particle spectra reflecting the nuclear temperature, the particle multiplicities provide an independent measure of the excitation energy E_ν^* of fragment ν :

$$E_\nu^* = \sum_{i=n,p,\alpha,\gamma} \langle E_{i\nu} + B_{i\nu} \rangle M_{i\nu}, \quad (1)$$

where $M_{i\nu}$, $E_{i\nu}$, and $B_{i\nu}$ are the multiplicity, kinetic energy, and binding energy of particle i from fragment ν . A complete experiment would require a measurement of all light particles including the

γ rays for both fragments, separately. However, since neutron emission is the dominant de-excitation channel, the neutron multiplicity represents an independent measure of the excitation energy requiring only approximate estimates for the corrections due to charged-particle and γ -ray emission.

Depending on the time scale on which light particles are emitted, there are three possible sources of these particles and thus three different frames of reference to consider. These sources are the intermediate double-nucleus complex and the two final fragments, fully accelerated by their mutual Coulomb field. It is the goal and also the main complication of the data analysis to identify the contributions from these sources. This is possible, in principle, by the use of the distinct features of particle emission in different processes. De-excitation particles from the final, fully accelerated fragments are likely to exhibit evaporationlike energy spectra and angular correlations determined by the velocities and emission angles of the fragments. Pre-equilibrium particles, on the other hand, are emitted on a short time scale and will reflect the kinematics of the double-nucleus complex. Depending on the physical processes producing these pre-equilibrium neutrons, different angular correlations and energy spectra will result. Fermi-jet or PEP² (promptly emitted particles) neutrons will be highly energetic with a maximum energy of ≈ 20 MeV for the reaction under investigation and will have a maximum intensity around the beam direction. However, highly energetic neutrons originating from a reaction mechanism described by the piston model³ will preferentially be emitted in the direction of the linear-momentum transfer. For the strongly damped part of the reaction, this corresponds approximately to the recoil-direction of the heavy fragment, whereas it is close to the beam direction for fusion-fission events.

There exists already some experimental evidence^{1,4} that the neutron-to-proton ratio (N/Z) of the final fragments from damped collisions equilibrates towards the N/Z of the composite system (1.38 in the present case). These observations are in accord with theoretical attempts⁵ to describe the relaxation of the N/Z degree of freedom which suggest a very short time constant ($\approx 10^{-22}$ s) for this process. A study of neutron emission adds to the information on this relaxation mechanism because the neutron multiplicities depend on the binding energies of the neutron and competing other light particles, and thus on the N/Z ratio of the emitting fragment. This dependence is particularly strong for the asymmetric system $^{165}\text{Ho} + ^{56}\text{Fe}$ studied in this work. The N/Z

ratios are very different for the nuclei in the entrance channel: 1.15 for ^{56}Fe and 1.46 for ^{165}Ho . In addition, the binding energies in the Fe region of the atomic mass table⁶ are very sensitive to the N/Z ratio. Hence, one expects a quite accurate determination of the pre-evaporation N/Z value from the measured neutron multiplicities to be possible for the Fe-like fragments produced at various stages of the reaction.

II. EXPERIMENTAL PROCEDURE AND DATA ANALYSIS

A. Experimental setup

The experiments were performed at the Lawrence Berkeley Laboratory SuperHILAC accelerator. Neutron and charged-particle emission was studied in the reaction $^{165}\text{Ho} + ^{56}\text{Fe}$ at 8.5 MeV/u bombarding energy, corresponding to 4 MeV/u of relative motion above the Coulomb barrier. Self-supporting ^{165}Ho targets were used with thicknesses of $435 \mu\text{g}/\text{cm}^2$ and $244 \mu\text{g}/\text{cm}^2$, in an initial overview experiment. A schematic setup of the experiment is shown in Fig. 1. The beam was dumped 4 m downstream from the target into a well-shielded graphite Faraday cup. Even though the beam was carefully kept off the collimator slits ahead of the scattering chamber, these slits were also shielded by a combination of iron bricks and water.

Six liquid-scintillator (NE213) detectors of dimensions $2.5 \text{ cm} \times 12.7 \text{ cm}$, $5.1 \text{ cm} \times 12.7 \text{ cm}$, and $3.8 \text{ cm} \times 10.2 \text{ cm}$ (thickness \times diameter) were used to detect the neutrons. In connection with these detectors highly efficient γ - n pulse-shape discrimination circuits⁷ were employed. In order to suppress low-energy γ rays and atomic x rays [$K_\alpha(\text{Ho}) = 47 \text{ keV}$], all scintillators were covered with 2-mm-thick Pb caps. A ΔE - E solid-state detector telescope subtending a solid angle of 22 msr was employed to measure the α particles. Another ΔE - E solid-state detector telescope subtending a solid angle of 4 msr was placed at selected angles to detect the projectilelike frag-

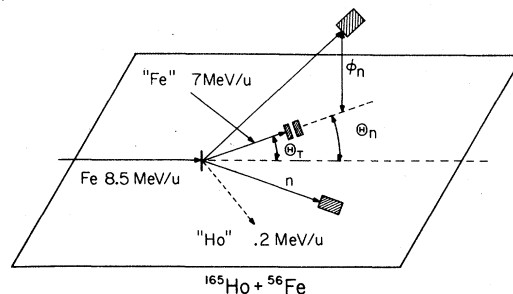


FIG. 1. Schematic diagram of the experimental setup.

ments in coincidence with neutrons and α particles.

For the final experiment the heavy-ion telescope was positioned at laboratory angles $\theta_T = 25^\circ$, 20° , and 16° . These angles are all forward of the grazing angle, $\theta_{gr} = 32.5^\circ$.⁸ The neutron detector angles θ_n were the same for all settings of θ_T and chosen as $25^\circ, 10^\circ, -10^\circ, -45^\circ, -70^\circ$ in the reaction plane ($\phi_n = 0$). One single neutron detector was placed out of the reaction plane at $\theta_n = 0^\circ$ and $\phi_n = 85^\circ$. The angle ϕ_n is defined as the angle between the reaction plane, determined by the heavy-ion telescope and the beam direction, and the neutron detector. Hence, the angle $\phi_n = 0$ corresponds to any direction in the reaction plane (see Fig. 1). The α telescope was positioned at $\theta_{LI} = 53^\circ$ and -57.5° .

The angles $\theta_n = 25^\circ, 10^\circ$ and $\theta_n = -45^\circ$ and -70° were used as master detector angles (cf. Sec. IIC) for the detected light and the correlated heavy fragments, respectively. The neutron detectors at $\theta_n = 10^\circ$ and -10° were located as close as possible to the beam direction in order to detect possible Fermi-jet neutrons. Although the fragment rest frames assumed in the lab-to-c.m. transformation (cf. Sec. IIC) do not apply to neutrons emitted from the composite complex, those should show up as highly energetic neutrons. However, the c.m. energies of Fermi-jet neutrons calculated by this procedure are somewhat over- or underestimated in the rest frame of the heavy or light fragment, respectively.

The neutron energy was determined with a time-of-flight method whereby the time difference between an event in the ion telescope and one in a neutron detector was measured. This time was corrected, event by event, for the fragment time of flight from the target to the ion telescope as deduced from the measured fragment Z and energy. The overall time resolution achieved for γ rays was typically 1 to 1.5 ns resulting in an energy resolution of 0.5 to 2 MeV for neutron energies between 5 and 10 MeV, for the flight path of 70 cm used in the experiment.

A typical time-of-flight spectrum of events identified as neutrons by the pulse-shape discrimination circuitry is shown in Fig. 2. The spectrum was recorded with a neutron detector placed at an angle of $\theta_n = 10^\circ$ in coincidence with the heavy-ion telescope at $\theta_T = 20^\circ$. The small peak on the left of the broad neutron time distribution is due to γ -ray events not rejected by the pulse-shape discrimination system. Favorable background conditions are demonstrated by the small number of events in the random-time range below 90 and above 170 ns.

For each event, 12 parameters were written on magnetic tape including the energy loss ΔE and

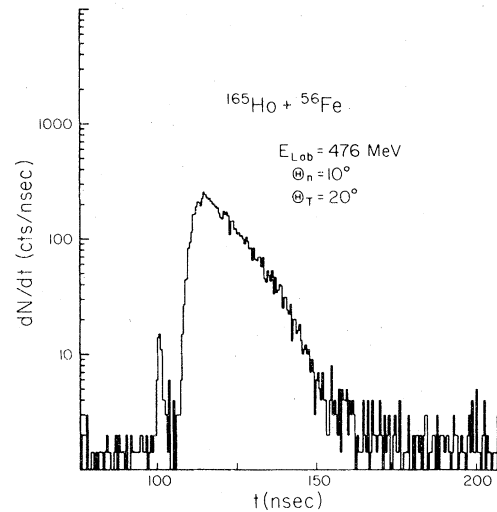


FIG. 2. Neutron time-of-flight spectrum. The small narrow peak at $t \approx 100$ ns corresponds to γ rays not rejected by the pulse-shape discrimination system.

the residual energy E of both the heavy-ion and the α -particle telescopes, the time difference between an event in the neutron detector or in the heavy-ion telescope, the proton recoil energy signal from each neutron detector, and an analogous signal which distinguished between the various neutron detectors and between neutrons and γ rays. This made it possible to mix the output signals of several neutron detectors into one parameter. An event was recorded only if the heavy-ion telescope E detector had fired.

The neutron detection efficiency was calculated with a computer code developed by Textor and Verbinski⁹ and checked against measured values of Drog.¹⁰ Calculated and experimental¹⁰ efficiencies agreed with each other within 5% for neutron energies between 2 and 10 MeV. The detection efficiency depends strongly on the threshold set on the proton-recoil energy. This threshold was, therefore, carefully adjusted to 1.08 or 0.5 MeV equivalent neutron energies^{11,12} using radioactive γ sources. This calibration was checked continuously during the experiment by comparing the neutron energies as determined by the time of flight and the proton recoil energy spectrum. In addition, tests were performed before and after the experiment in which neutrons from ^{252}Cf fission fragments were measured in a geometry similar to that of the data-taking runs. Including the uncertainty of the neutron threshold, the accuracy of the absolute neutron efficiency was estimated to be approximately 10%.

Calculations, as well as test measurements with ^{252}Cf fission neutrons¹³ indicated that neutrons

produced in the target and scattered off the walls of the scattering chamber in the initial setup posed serious background problems, and very large corrections were necessary due to neutron in and out scattering. In order to reduce this background, a thin (3.2 mm) stainless-steel shell was designed for the scattering chamber (76 cm diameter). The resulting attenuation of the neutron flux was calculated to amount to 8% and 4% for neutron energies of 4 and 14 MeV, respectively. Furthermore, all mounts of the solid-state detector telescopes were made as light as possible. The massive base of the chamber gave rise to delayed γ rays from (n, γ) processes in aluminum, which could be clearly identified in the γ -time distribution, emphasizing the importance of an efficient γ - n pulse-shape discrimination in such experiments. These events, if not identified as γ rays, would have been mistaken as highly energetic neutrons.

B. Complete angular distributions

In order to identify the major neutron emitters, complete in-plane and out-of-plane angular distributions were measured for neutrons in coincidence with the reaction fragments detected at a laboratory angle $\theta_T = 23^\circ$. The detection threshold was set at 0.5 MeV neutron energy in this case. Figures 3 and 4 show the angular dependence of the neutron cross section and of the mean neutron energy $\langle E_n \rangle$, respectively, for damped reaction

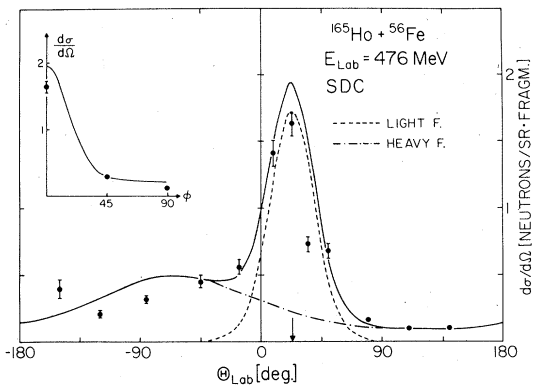


FIG. 3. Angular distributions of the neutron intensity in the laboratory system for strongly damped collisions (SDC) where Z of the detected fragment is between 10 and 29. The heavy-ion telescope was located at an angle of 23° (vertical arrow). The dashed and dashed-dotted curves are the results of an evaporation calculation [Eq. (A4)] for the light and heavy fragment, respectively, averaged over all values of E_{loss} . The solid line is the sum of the calculated intensities of the two fragments. The insert shows the out-of-plane distribution measured at $\theta_n = 25^\circ$.

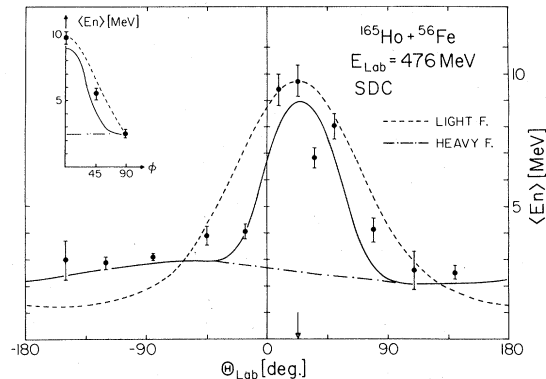


FIG. 4. Angular distribution of the mean neutron energy [Eq. (A6)] in the lab system for strongly damped collisions (SDC). The dashed, dashed-dotted, and solid curves are the results for the light fragment, heavy fragment, and the weighted average of both, respectively.

fragments with $10 \leq Z \leq 29$, integrated over total kinetic-energy loss. As can be seen from Fig. 3, there is a clear concentration of the neutron intensity at the scattering angle of the projectile-like fragment indicated by the vertical arrow ($\theta_T = 23^\circ$). At this angle the neutrons have also the highest mean kinetic energies as shown in Fig. 4. However, tails of the neutron angular distribution corresponding to significantly lower neutron energies (i.e., Fig. 4) extend to large angles on both sides of the recoil direction. They are due to neutrons from the corresponding heavy fragment moving with considerably smaller velocities (0.2 MeV/u) than the Fe-like fragment (5–7 MeV/u). The dashed and dashed-dotted curves shown in Figs. 3 and 4 are the results of an evaporation calculation using Eqs. (A4) and (A6) of the Appendix, respectively. The assumption made in this calculation implies an essentially isotropic emission of neutrons from the fully accelerated fragments in the fragments' rest frames. Obviously the data are in reasonable agreement with the solid curve accounting for the contributions from both the heavy and light fragments. The inserts in Figs. 3 and 4 show the variation of the respective quantities with the out-of-plane angle ϕ which was defined previously. In Fig. 5, the respective angular distributions are shown for the fusion-fission part of the reaction, i.e., $30 \leq Z \leq 55$.

From these results one concludes that the neutrons are, indeed, predominantly emitted from the fully accelerated fragments. Supported by this observation, laboratory neutron energies and intensities were transformed into the rest frames of the fully accelerated light and heavy fragments. Any deviation from this assumption is then detect-

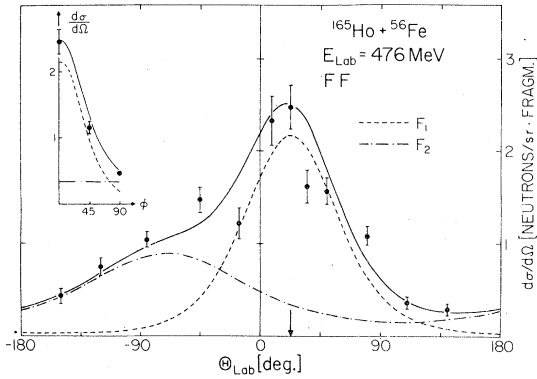


FIG. 5. Angular distribution of neutrons emitted from fusion-fission (FF) fragments F_1 and F_2 ($30 \leq Z \leq 55$). See also figure caption of Fig. 3.

able in a comparison of the center-of-mass neutron intensities and energies at different neutron detection angles, each of these angles having a different sensitivity to neutrons from either of the two separated fragments or from the composite complex.

C. Data analysis

In the lower part of Fig. 6, the double-differential neutron cross sections for the detected light (solid lines) and the correlated heavy frag-

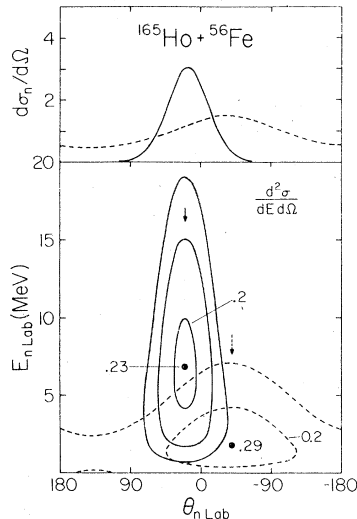


FIG. 6. In the lower part of the figure, the double-differential cross section ($d^2\sigma/dE d\Omega$) in the lab system [Eq. (A3)] is plotted in a contour diagram versus neutron detection angle and energy. The light (solid line) and heavy fragments (dashed line) are scattered to 20° and -40° , respectively. In the upper part of the figure, respective cross sections integrated over the neutron energy are depicted. A large E_{loss} value of 200 MeV has been used to generate the distributions.

ments (dashed lines) are shown for a total kinetic energy loss E_{loss} of 200 MeV in a contour diagram plotted versus the neutron detection angle and the neutron laboratory energy. The respective scattering angles of the two fragments are indicated by the vertical arrows. This two-dimensional plot demonstrates very clearly the separation in energy and emission angle of neutrons emitted from the two sources. In fact, for total kinetic energy losses smaller than 200 MeV corresponding to partially damped events, the separation is considerably better than indicated in Fig. 6. Because of this good separation it is possible to use not only the emission angle but also the neutron lab energy as indications of the origin of the detected neutrons. In the following, the neutron detector angles in the direction of the light- and heavy-fragment scattering angles are denoted as the master angles for neutrons from the light and heavy fragments, respectively. At these angles, the intensity of neutrons from one fragment is the dominant part of the measured spectrum, whereas the contribution from its reaction partner is small (see Fig. 6).

For each neutron event in any of the neutron detectors located at angles θ_n and ϕ_n , the factors $f_\nu(E_n, \theta_n, E_\nu, \theta_\nu, m_\nu)$ applying to the transformation from the lab to the c.m. system were calculated for both fragments. Here $m_\nu = (A/Z)Z + \delta m_\nu$ is the pre-evaporation mass of fragment ν . The quantities E_ν , θ_ν , and δm_ν are the measured energy, angle, and calculated evaporated mass, respectively, of the light fragment ($\nu=L$) or the correlated heavy fragment ($\nu=H$). In order to determine the mass of the detected fragment, it was assumed that its A/Z ratio was that of the valley of β stability. With these transformation factors, the double differential cross section for neutrons from fragment ν becomes

$$\left(\frac{d^2\sigma_\nu}{d\Omega dE} \right)_{\text{c.m.}} = f_\nu C_\nu \left(\frac{d^2\sigma}{d\Omega dE} \right)_{\text{lab}}, \quad (2)$$

where C_ν is a correction factor accounting for the contribution from the respective correlated fragment. For events with total kinetic energy losses of 200 MeV and 50 MeV this correction amounts to 30% and 7%, respectively, at the light-fragment master angle, and 5% to 1%, respectively, at the heavy-fragment master angle. Hence, at these angles the final results are largely independent of the assumption used to calculate C_ν .

The correction factors C_ν were calculated assuming evaporative neutron spectra and isotropic emission in the rest frame of each fragment. For a given angle, this results in a ratio R for the yields of neutrons of energy E_n from the heavy and light fragments given by

$$R = (M_H/M_L)(E_{c.m.}^H/E_{c.m.}^L)^{1/2} \times \exp[-E_{c.m.}^H/T_H + (E_{c.m.}^L/T_L)], \quad (3)$$

where M_ν , $E_{c.m.}^\nu$, and T_ν are the neutron multiplicity, neutron c.m. energy, and nuclear temperature of fragment ν , respectively. The value of $E_{c.m.}^\nu$ is calculated using the laboratory neutron energy E_n and the respective fragment velocity. With this ratio R one obtains $C_L = 1/(1+R)$ and $C_H = R/(1+R)$. Relation (3) results in $\langle R \rangle \ll 1$ or $\langle R \rangle \gg 1$ for the master angle of the light or heavy fragment, respectively, yielding $\langle C_\nu \rangle \approx 1$ in both cases. This indicates again that the results obtained for the master angles are largely independent of the details used to calculate R .

Values of the ratio M_H/M_L and of the temperatures T_H and T_L have to be specified as starting parameters for an iterative analysis of the data. In the procedure applied here, M_H/M_L was initially set equal to the fragment mass ratio m_H/m_L calculated event by event as described above, and the total excitation energy was distributed in proportion to the fragment masses. This implies that $T_H = T_L \propto (E_{\text{loss}})^{1/2}$ was assumed as an initial condition in the iterative procedure. One can then use the results of the first event tape replay for M_H/M_L and T_H/T_L as input parameters for the second iteration. However, the final results were largely independent of these assumptions and very close to the situation described above. It was, therefore, not necessary in most of the analyses to make a second iteration.

In order to test quantitatively the event analysis described above with respect to the sensitivity of the final result to the nuclear temperatures and neutron multiplicities, a test program was used to generate synthetic neutron spectra. For instance, various spectra were analyzed corresponding to ratios T_H/T_L and $(M_H/M_L)(m_L/m_H)$ ranging from $\frac{1}{3}$ to 3. In each case the analysis gave results within a few percent of the correct temperatures and multiplicities of the test spectrum.

III. EXPERIMENTAL RESULTS AND DISCUSSION

A considerable amount ($\approx 25\%$) of the total reaction cross section of the reaction $^{165}\text{Ho} + ^{56}\text{Fe}$ at the bombarding energy of 476 MeV is associated with fusion-fission leading to an average fragment Z of about 46 corresponding to symmetric fission of the composite system. In comparison, the strongly damped part of the reaction cross section is concentrated around $Z = 26$ (Fe) with respect to the detected light fragment. No contribution from sequential fission of the targetlike nucleus was observed. In the following, the strongly damped part of the reaction is defined by the requirement

$20 \leq Z \leq 30$ and fusion-fission corresponds to $35 \leq Z \leq 55$.

A. Nuclear temperatures of the strongly damped reaction fragments

In Fig. 7 the c.m. neutron energy spectra in the rest frames of the light (open circles) and heavy (filled squares) fragments are shown for all six neutron detector angles. The data are weighted averages over all three telescope angles $\theta_T = +16^\circ$, 20° , and 25° and total kinetic energy losses larger than 36 MeV. The error bars depicted include only statistical errors and do not account for the uncertainty of the neutron detection efficiency and background subtraction which become appreciable at high neutron energies. This makes the results above $E_{c.m.} \approx 10$ –15 MeV considerably more uncertain than indicated by the error bars. The interpretation of high-energy parts of the neutron spectra is further complicated by the deterioration of the neutron energy resolution at high energies (≈ 4 MeV at $E_n = 20$ MeV). The solid curves are calculated evaporation spectra with a temperature of 2 MeV [see Eq. (A1) with $\eta = 0.5$] normalized to the spectra at the master angles for the light fragment at 25° and 10° and for the heavy fragment at -45° and -70° (heavy solid lines).

In addition to the neutron energy cutoff due to the detection threshold (1.08 MeV), there is also a kinematical cutoff, if a neutron detector is not aligned with the recoil direction of the respective fragment, due to the strong focussing of low-energy neutrons into the recoil direction. This effect causes the low-energy falloff of the $\theta_n = -45^\circ$ neutron spectrum for $E_{c.m.} \leq 5$ MeV in the case of neutrons associated with light fragments (see Fig. 7).

As has been discussed previously (cf. Sec. IIC), the results obtained for the master angles are largely independent of the specific assumptions made in performing the analysis. Inspecting these energy spectra closely, one observes that, with the exception of very high $E_{c.m.}$, the spectra corresponding to light and heavy fragments have approximately the same exponential decrease. Since the slope of the neutron spectrum reflects the nuclear temperature of the emitting fragment, one arrives at the important conclusion that the temperatures of the light and heavy fragment must be similar. Furthermore, the contribution of high-energy pre-equilibrium neutrons appears to be small, as can be inferred from the high-energy parts of these spectra. Integrating the neutron intensity in excess of the evaporation spectrum results in an upper limit of 5% of a possible contribution of pre-equilibrium neutrons. Assuming,

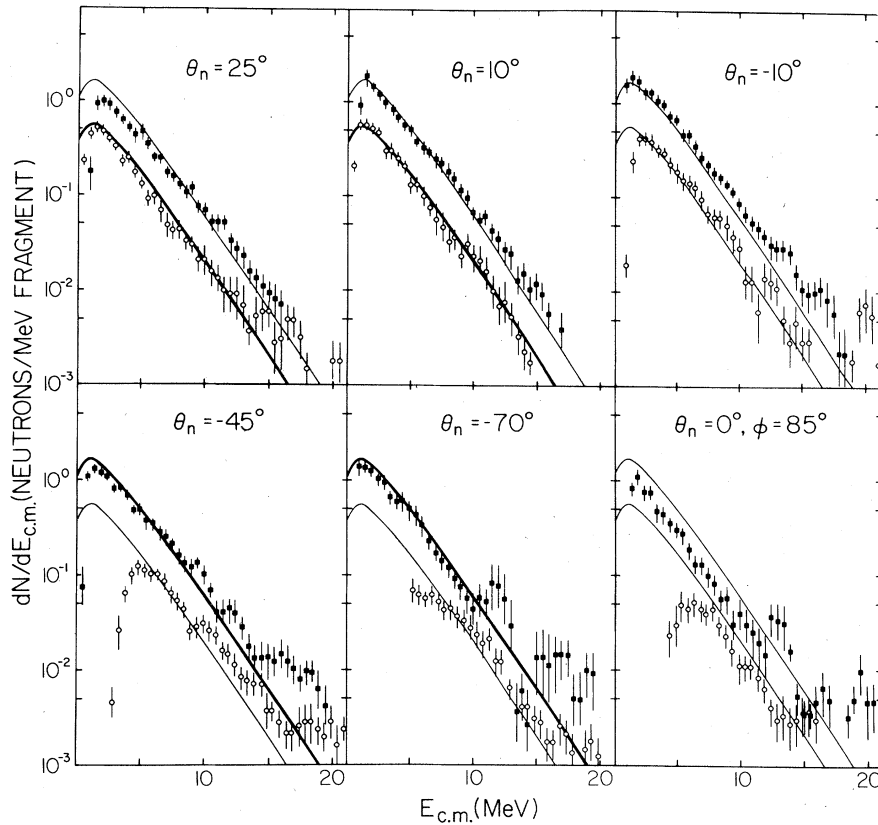


FIG. 7. Neutron energy spectra in the rest frames of the light (open circles) and the heavy (filled squares) fragments for all neutron detector angles. The spectra were averaged over Z between 20 and 30, E_{loss} values larger than 36 MeV, and all three settings of the telescope angle $\Theta_T = 16^\circ, 20^\circ,$ and 25° . The solid lines represent evaporation spectra $dN/dE = \sqrt{E} e^{-E/T}$ and are normalized to the experimental points at 25° and 10° for the light fragment (open circles) and at -45° and -70° for the heavy fragment (filled squares).

furthermore, that a pre-equilibrium contribution is associated only with the first neutron of each cascade, one has to multiply the above result with the average neutron multiplicity. This results in an upper limit of 25% for the probability for the first neutron to be emitted by the heavy fragment in a pre-equilibrium process. However, including a reasonable estimate for the systematic errors mentioned above, the high-energy points are almost consistent with the evaporation spectra given in Fig. 7. This assigns a low confidence level to the value deduced for the upper limit of the pre-equilibrium neutron emission probability.

The most forward neutron detectors at $\theta_n = \pm 10^\circ$ should be specifically sensitive to highly energetic neutrons from the Fermi-jet mechanism. However, the spectra show almost no contribution from highly energetic neutrons at these angles, thus providing no support for this emission mechanism.

The energy spectra of Fig. 7 have been averaged

over all values of E_{loss} larger than 36 MeV and hence yield information only about the average degree of energy equilibrium. However, most significant for an understanding of the equilibrium mechanism appears to be its evolution as the interaction time proceeds. Adopting the assumption¹⁴ that the interaction time depends monotonically on the E_{loss} , it is possible to infer the progress of energy equilibration with time by measuring the fragment temperatures as a function of E_{loss} . The experimental dependence of the temperature on energy loss is shown in Fig. 8. According to the evolution of interaction times mentioned above, an E_{loss} of 100 MeV corresponds^{1,8} to an interaction time of either ≈ 4 or $\approx 8 \times 10^{-22}$ s assuming the non-sticking or sticking situation, respectively. One observes that the temperatures deduced from the c.m. neutron energy spectra of the master angles are, within the experimental uncertainty, the same for both fragments already for interaction times as short as $\approx 5 \times 10^{-22}$ s. Furthermore, the

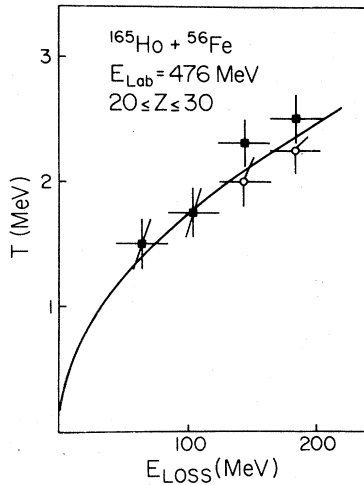


FIG. 8. Nuclear temperature as a function of the E_{loss} for the light (open circles) and heavy (filled squares) fragments. The solid curve represents the calculated nuclear temperature $T = \frac{11}{12} (E_{\text{loss}}/a_{CN})^{1/2}$ with $a_{CN} = [(A_P + A_T)/8]$ MeV^{-1} being the level density parameter of the composite system.

points follow closely the theoretical curve representing the Fermi-gas relation between temperature and excitation energy assuming that the entire loss is converted into intrinsic excitation and the level density parameter to be given by $a = (A/8)$ MeV^{-1} . LeCouteur and Lang¹⁵ have derived an effective temperature $T = \frac{11}{12} (E^*/a)^{1/2}$ for a neutron cascade, where E^* is the initial excitation energy. This relation is shown by the curve in Fig. 8. Although the limited accuracy of the data does not allow firm conclusions in this respect, the results are consistent with the assumption that the intrinsic-excitation energy E^* is given by the measured E_{loss} of the asymptotic fragment kinetic energies, a quantity that may, conceptually, be different from the amount of kinetic energy that is irreversibly dissipated into intrinsic degrees of freedom.

In concluding this section, it is emphasized again that the observation of equal temperatures for light and heavy fragments suggests strongly that nearly complete equilibration of the excitation energy is reached in a damped heavy-ion collision already for interaction times as short as 5×10^{-22} s.

B. In-plane and out-of-plane correlation

The fact that the experimental neutron spectra obtained for both fragments at various angles in the reaction plane agree so well in shape and magnitude with the spectra measured at the master angles is consistent with a process where neu-

trons are emitted isotropically in the rest frames of the fully accelerated fragments. However, so far this has only been established for neutrons emitted in the reaction plane. In fact, the assumption of isotropic emission leads to disagreement with the out-of-plane data as shown in Fig. 7 for $\theta_n = 0^\circ$ and $\phi_n = 85^\circ$, corresponding to an emission angle of approximately 90° in the rest frame of the heavy fragment. The experimental points lie systematically below the evaporation spectra (curves) deduced from the spectra measured at the master angles. From this one obtains an out-of-plane anisotropy

$$A_2 = \left[\frac{d\sigma}{d\Omega}(\phi = 0^\circ) / \frac{d\sigma}{d\Omega}(\phi = 90^\circ) \right] - 1$$

of 0.2 ± 0.1 for neutrons from the heavy fragment. The intensity of neutrons from the light fragment measured at this angle cannot be used to extract an independent value of A_2 for the light fragment because it is strongly dependent on the specific assumptions made in the analysis.

According to the theory of Ericson and Strutinsky,¹⁶ the out-of-plane angular correlation W of particles evaporated from a nucleus with temperature T and moment of inertia j is a function of the spin I of the nucleus and the angular momentum l carried away by a particle:

$$W(\phi) \approx 1 + \frac{1}{2} \left(\frac{\hbar^2}{2jT} \right)^2 \langle I^2 \rangle \langle l^2 \rangle \cos^2 \phi, \quad (4)$$

where $\langle I^2 \rangle$ and $\langle l^2 \rangle$ are the mean-squared values corresponding to the normal of the scattering plane. Assuming a rolling or sticking situation in the collision, typical values of the asymmetry are estimated to amount to 4% or 12%, respectively, in qualitative agreement with the experiment. However, since the angular momentum l carried away by a nucleon evaporated from a spherical nucleus is small ($1\hbar$ to $2\hbar$ in the present case), the measurement of the out-of-plane angular correlation does not provide as sensitive a test of the fragment alignment as would be possible with heavier particles.

C. Neutron multiplicities

As has been pointed out in Sec. I [cf. Eq. (1)], the neutron multiplicity also measures the excitation energy, although somewhat indirectly. The experimental neutron multiplicities for the light (open circles) and heavy (filled squares) fragments are plotted in the lower part of Fig. 9 versus the measured atomic number Z_L of the detected fragment and that of the correlated heavy fragment assumed to be given by $Z_H = Z_T + Z_P - Z_L$. The measured fragment Z values have not been cor-

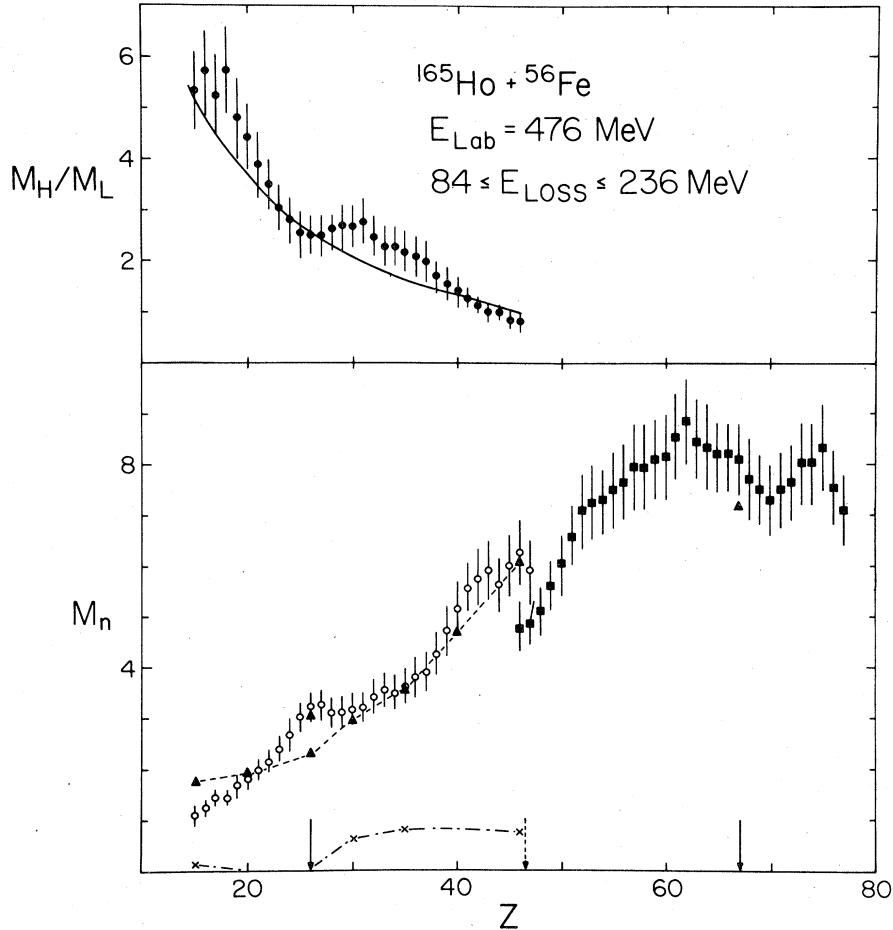


FIG. 9. Neutron multiplicities M_L (open circles) and M_H (filled squares) are shown as functions of Z_L and $Z_H = Z_P + Z_T - Z_L$, respectively (see text). The filled triangles and crosses are the results of evaporation calculations (Ref. 17) for neutron and charged-particle ($p + \alpha$) emission, respectively. In the upper part of this figure the ratio M_H/M_L is plotted and compared to the mass ratio m_H/m_L (solid line).

rected for possible charged-particle evaporation since no accurate experimental data are available. As shown in Fig. 9 the multiplicities increase approximately linearly with increasing atomic number or mass of the fragment. At $Z \approx 46$ (dashed vertical arrow) a discontinuity appears between the multiplicities deduced for the detected (open circles) and the correlated (filled squares) fragments, although they should be equal for the symmetric-fission fragments. This discrepancy can be understood in terms of charged-particle emission from these fragments. Using the evaporation code of Beckerman and Blann,¹⁷ one obtains a charged-particle (protons and α particles) multiplicity of ≈ 0.75 (indicated by the crosses in Fig. 9) or an average evaporated charge of 1.25 per fragment, for fragments with $Z \approx 46$. This is in qualitative agreement with approximate α -particle

measurements performed in this work yielding an estimate for $M_\alpha \approx 0.5 - 1.0$ for fusion-fission fragments. If then a correction is applied accounting for charged-particle emission, the circles and squares have to be moved to the right and left on the Z axis, respectively, by 1.25 units each, resulting in a smooth transition between the two sets of data. The mean neutron multiplicity obtained for the fusion-fission fragments is $M_n = 5.7 \pm 0.7$ (see Table I).

Also shown in Fig. 9 are the results of an extensive evaporation calculation using the code MBII¹⁷ (filled triangles and crosses). The dashed and dashed-dotted curves are drawn through the calculated points. The basic assumption for the parameters used in the calculation were (1) the excitation energy was taken to be apportioned according to the mass ratio, (2) the binding energy

TABLE I. Mean neutron multiplicities and neutron energies.

θ_T	$\langle E^* \rangle^a$ (MeV)	$\langle M_L \rangle^b$ $\pm 10\%$	$\langle E_L \rangle^c$ (MeV)	$\langle M_H \rangle^b$ $\pm 10\%$	$\langle E_H \rangle^c$ (MeV)	$\langle M_{tot} \rangle$ $\pm 10\%$	$\langle E_R \rangle^d$ (MeV) $\pm 15\%$	Reaction ^e
16°	113	1.93	3.1	5.77	3.1	7.69	27.5	SDC
20°	100	2.02	3.0	5.59	3.1	7.65	15.2	SDC
25°	83	1.56	2.4	4.01	2.5	5.57	20.7	SDC
(16, 20, 25)	224	5.7	3.6	5.7	3.6	11.4	88	FF

^a $\langle E^* \rangle = \langle E_{loss} \rangle + \langle Q_{gg} \rangle$ weighted mean with $E_{loss} > 36$ MeV.

^b Weighted-mean neutron multiplicity with $E_{loss} > 36$ MeV.

^c Weighted-mean first moment of c.m. neutron energy spectrum.

^d Residual excitation energy that is not carried away by neutron emission.

^e SDC: $20 \leq Z_L \leq 30$. FF: $35 \leq Z_L \leq 55$.

of the first evaporated particle was assumed corresponding to a completely equilibrated ratio N/Z ($= 1.38$), and (3) the angular momentum used was estimated from the sticking limit for two touching spherical nuclei. The excitation energy was calculated from the average value of E_{loss} and the ground-state Q value Q_{gg} . Within the experimental errors and the uncertainty of the evaporation calculation (estimated to be 10–20%), one obtains very good agreement with the measurements, except around $Z = 26$ and $Z = 67$ (solid vertical arrows) corresponding to the projectile and target Z , respectively. Here, however, the assumption of the sticking limit is not very realistic. By decreasing the angular momentum of the light fragment from $17\hbar$ to $11\hbar$, more thermal energy (≈ 5 MeV) is available for neutron evaporation and less for γ -ray emission. This results in an increased multiplicity represented by the upper triangle for $Z = 26$, as is shown in Fig. 9. Although there are no γ -ray multiplicity measurements available for the system $^{165}\text{Ho} + ^{56}\text{Fe}$, a similar effect has been observed by Aleonard *et al.*¹⁸ for the dependence of the γ -ray multiplicity on the fragment atomic number in the reaction $^{165}\text{Ho} + ^{86}\text{Kr}$ at 618 MeV, which has a pronounced minimum at the projectile Z . Physically, this implies a close relation between the number of transferred particles which deposit their relative linear momentum and the transferred angular momentum.

In Fig. 9, the crosses connected by a dashed-dotted line represent the results of the calculation for the charged-particle multiplicities $M_{p+\alpha}$. The fact that charged-particle emission from fragments around $Z \approx 26$ is quite improbable is directly tied to the binding-energy assumption (2) listed above. This assumption is discussed in more detail below.

In the upper part of Fig. 9, the ratio M_H/M_L of the neutron multiplicities for the light detected fragment (M_L) and the heavy correlated fragment

(M_H) are plotted as a function of Z_L . The solid curve represents the mass ratio m_H/m_L deduced from the measured Z_L assuming $N/Z = 1.38$, i.e., N/Z of the composite system. Within the experimental error bars, good agreement with the relation $M_H/M_L = m_H/m_L$ is obtained.

Neglecting γ -ray emission this ratio is given to first approximation by

$$M_H/M_L = \frac{E_H^* \langle E_n + B_n \rangle_L}{E_L^* \langle E_n + B_n \rangle_H} \times \frac{[(\Gamma_p/\Gamma_n) + (\Gamma_\alpha/\Gamma_n) + 1]_L}{[(\Gamma_p/\Gamma_n) + (\Gamma_\alpha/\Gamma_n) + 1]_H}, \quad (5)$$

where E_ν^* , E_n , B_n , and Γ_i stand for the excitation energy of fragment ν , the mean kinetic energy carried away per neutron [$E_n = 1.5T$, see Eq. (A2), $n = 0.5$], the neutron binding energy and the evaporation width for particle i , respectively. Since (Γ_p/Γ_n) and (Γ_α/Γ_n) are sensitive to the difference of binding energies ($B_{p,(\alpha)} - B_n$) and thus the N/Z ratio, the third term also depends sensitively on the pre-evaporation N/Z ratio. The use of assumption (2) given above, results in a very small amount of charged-particle emission from either fragment and approximately equal binding energies B_{nL} and B_{nH} for the system under investigation. With the above statement and the equal-temperature relation, Eq. (5) can be written as

$$M_H/M_L \approx E_H^*/E_L^* \approx a_H T_H^2 / a_L T_L^2 \approx m_H/m_L, \quad (6)$$

where a_ν is the level density parameter $a_\nu = A_\nu/8$. Consequently, observing a relation $M_H/M_L = m_H/m_L$ is consistent with a full equilibration of the excitation energy degree of freedom during the interaction time.

The neutron multiplicities shown in Fig. 9 are averages over all values of E_{loss} above 86 MeV with an average E_{loss} of ≈ 160 MeV corresponding to an average interaction time of $(8 \text{ or } 17) \times 10^{-22}$ s assuming a nonsticking or sticking situation, re-

spectively. It is again possible to obtain information about the time scale on which the excitation-energy degree of freedom equilibrates using the relation between energy loss and interaction time discussed previously.¹ For this purpose the neutron multiplicities for the light fragment ($20 \leq Z_L \leq 30$) and the correlated heavy fragment ($73 \geq Z_H \geq 63$) are plotted versus E_{loss} in Fig. 10(a). As shown in this figure, the neutron multiplicities increase almost linearly with E_{loss} increasing up to 120 and 180 MeV for the light and heavy fragment, respectively. Furthermore, up to these energies the experimental results agree very well with the evaporation calculations (solid triangles) connected by the dashed line in Fig. 10(a) assuming N/Z equilibration. That is, provided that this assumption is true, one can conclude from the ob-

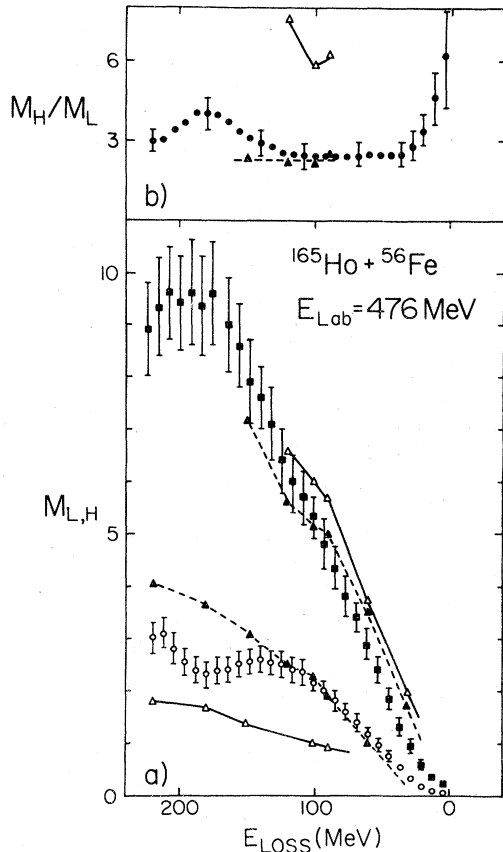


FIG. 10. (a) Neutron multiplicities M_L (open circles), M_H (filled squares), and (b) the ratio M_H/M_L (filled circles) are plotted versus E_{loss} for $20 \leq Z \leq 30$. The open and filled triangles represent evaporation calculations (Ref. 17) for M_L , M_H , and M_H/M_L assuming an N/Z value corresponding to the valley of β stability and a value equilibrated towards N/Z of the composite system, respectively. The solid and dashed lines in (a) and (b) are drawn through the calculated points to guide the eye.

served dependence of neutron multiplicities on E_{loss} , that the excitation energy is equilibrated for values of E_{loss} as small as 60 MeV corresponding to very short interaction times. This is consistent with the results given above for the nuclear temperatures.

However, there is a considerable discrepancy between the evaporation calculations and the experimental results for large energy losses, especially for the light fragment with values of E_{loss} above 120 MeV. This may be due to a considerable transfer of angular momentum in collisions damped to the Coulomb energy of spherical fragments or below. In the calculations it was assumed that the maximum possible fraction of the angular momentum corresponding to the rolling limit had been dissipated for an E_{loss} of 130 MeV, decreasing linearly towards an E_{loss} of zero and remaining constant for larger values of E_{loss} . Such a dependence has been derived from γ -ray multiplicity measurements by Olmi *et al.*¹⁹ although for a different system, and is expected from the angular-momentum dissipation theory of Wolschin and Nörenberg.²⁰ Possible larger amounts of angular momentum transferred would lead to a decreasing neutron multiplicity, since collective rotational energy is not available for particle emission.

The discrepancy discussed above may also be due to an N/Z equilibration process which is retarded or damped at high temperatures, a possibility which will be discussed below. However, in order to attribute the deviation of the neutron multiplicities from the results of the evaporation calculations at high values of E_{loss} uniquely to either of the above effects, a more complete experiment is necessary in which all emitted particles, including protons and α particles as well as γ rays are measured.

In Table I, the measured average neutron multiplicities, neutron energies and E_{loss} values given for strongly damped collisions (SDC) and the fusion-fission (FF) part of the reaction cross section. Column 8 of Table I lists the average residual energy E_R , which is not carried away by neutrons but must go into p , α , and γ -ray emission.

Finally, a quantity of practical interest is the total neutron production cross section $\sigma_{n,\text{tot}}$. This quantity has been derived from the total kinetic energy loss spectrum⁸ of the reaction $^{165}\text{Ho} + ^{56}\text{Fe}$ and the dependence of the total neutron multiplicity on the value of E_{loss} . For the reaction $^{165}\text{Ho} + ^{56}\text{Fe}$ at 476 MeV bombarding energy, a value of $\sigma_{n,\text{tot}} = 26.7 \pm 3 \text{ b}$ is obtained. Similarly large neutron production cross sections have resulted from the pioneering experiment of Broek²¹ who reported neutron production cross sections of 2.8 and 25 b

in the reaction of 160-MeV oxygen on targets between aluminum and gold, respectively.

D. N/Z equilibration

Since the largest fraction of the energy carried away per emitted neutron is given by the neutron binding energy B_n , the total number of emitted neutrons for a given excitation energy is almost directly proportional to B_n . By increasing the neutron-to-proton ratio of a given nucleus, the neutron binding energy decreases whereas the proton binding energy increases. Hence, the probability of charged-particle emission is drastically reduced for an increasing N/Z ratio, since

$$\Gamma_n / \Gamma_{p,(\alpha)} \propto \exp[(B_{p,(\alpha)} - B_n) / T],$$

where $B_{p,(\alpha)}$ is the binding energy of protons and α particles including their respective Coulomb barriers. The α -binding energy has a weak N/Z dependence. Both effects amplify the sensitivity of the neutron multiplicity as a probe for the N/Z ratio. Since an increase in the N/Z ratio of the projectilelike fragment implies a decrease of N/Z of the targetlike fragment, the sensitivity of the ratio M_H/M_L to the neutron-to-proton ratio is further enhanced, as can be seen from Eq. (5). Furthermore, in this ratio the dependence of M_p on the total transferred angular momentum cancels, to first approximation.

In Fig. 11 the results of the evaporation calculation for the ratio M_H/M_L are plotted versus the neutron-to-proton ratio of the projectilelike fragments ($20 \leq Z_L \leq 30$). The error bars given represent uncertainties of the calculation. The excitation energy has been assumed to be apportioned according to the mass ratio, as discussed earlier. The hatched area represents the experimental value M_H/M_L at an E_{loss} of 100 MeV. Obviously, the data are consistent with values of N/Z larger than 1.26 up to the N/Z equilibration value of the composite system ($N/Z = 1.38$).

Until now the equilibrium N/Z ratio has implicitly been identified with the N/Z ratio of the composite system. This is *a priori* a model-independent definition. The equilibrium neutron-to-proton ratio for a given charge division (Z_1, Z_2) and an angular momentum l of the interacting system with a given shape is defined by the minimum potential-energy surface $V_l(Z_1, N_1, Z_2, N_2)$ with respect to a variation in (N_1/N_2). This potential surface has been approximated using the liquid-drop model.²² Coulomb point charges and rotational energies are given by those of two nuclei at a separation distance equal to the strong-absorption radius or the sum of the two nuclear radii. These calculations accounting for shell corrections

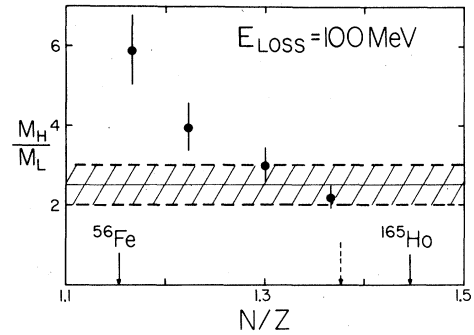


FIG. 11. The calculated ratio M_H/M_L of the neutron multiplicities M_L and M_H of the light and heavy fragments, respectively, is plotted versus N/Z of light fragment with $20 \leq Z_L \leq 30$ and $E_{\text{loss}} \approx 100$ MeV. The hatched area represents the experimental value of M_H/M_L . The vertical dashed arrow indicates the N/Z value of the composite system, whereas the solid arrows show those of ^{56}Fe and ^{165}Ho .

result in an equilibrium N/Z ratio of 1.30 for $l = 0$ and $20 \leq Z_L \leq 30$, in agreement with a value of 1.31 obtained using the maximum ground-state Q_{gr} values as deduced from the mass tables.⁶ For a value of E_{loss} of 100 MeV, the average initial angular momentum⁸ is $l = 193\hbar$. In this case, one obtains 1.39 or 1.49 for the equilibrium N/Z value, depending on whether the strong absorption radius or the sum of the nuclear radii is used for the separation distance of the ions, respectively. Hence, for $l = 193\hbar$ the model predicts the equilibrium N/Z value to be slightly larger than that of the composite system (1.38). Both predictions for the equilibrium N/Z values are consistent with the present experimental result at an E_{loss} of 100 MeV.

In Figs. 10(a), 10(b) the neutron multiplicities M_H and M_L and their ratios are compared with the evaporation calculations, assuming either $N/Z = 1.15$ (open triangles) or $N/Z = 1.38$ (filled triangles) for the projectilelike fragment. Here, too, it is clear that the data are consistent with N/Z equilibration towards N/Z of the composite system for energy losses between 80 and 120 MeV. The evaporation calculations become very uncertain for excitation energies close to the binding energy of one neutron. Hence, it is not feasible to perform an unambiguous comparison with the data at smaller total kinetic energy losses. Thus, with this method it is not possible to deduce the N/Z ratio for fragments with values of E_{loss} smaller than 80 MeV.

For the light fragment with energy losses above 120 MeV, the experimental multiplicities assume values in between the predictions based on either assumption made on the N/Z ratio. This could be

interpreted as a different mechanism of N/Z equilibration at low angular momenta corresponding to large values of E_{loss} or high temperatures resulting in a damping of this equilibration. However, since the present data are not complete, it is possible that this deviation is due to a transfer of amounts of angular momentum larger than assumed to the light fragment, at large values of E_{loss} .

Summarizing the results discussed in this section, one may conclude that the neutron-to-proton ratio is almost equilibrated at interaction times as short as $(4 \text{ or } 8) \times 10^{-22} \text{ s}$, depending on a non-sticking or sticking situation, respectively. Brosa and Krappe⁵ have predicted N/Z equilibration to be achieved within times of $\approx 2 \times 10^{-22} \text{ s}$ for the system $^{165}\text{Ho} + ^{56}\text{Fe}$ assuming the mass-to-charge equilibration mode to be not overdamped. This is consistent with the present results.

IV. CONCLUSIONS

Summarizing the results of this investigation, it is found that the excitation-energy degree of freedom and the neutron-to-proton ratio are equilibrated on the very short time scale of $(5-10) \times 10^{-22} \text{ s}$. Neutrons are emitted from the fully accelerated fragments, that is, after $\approx 5 \times 10^{-21} \text{ s}$. Very few, if any, events are observed with a signature of pre-equilibrium processes. The data provide no evidence for Fermi-jet neutrons.

Very similar results, with respect to equilibration of the excitation energy, have been obtained in other investigations²³⁻²⁹ using a variety of different methods. All those investigations using neutron emission directly or indirectly as an indication for pre-equilibrium effects are summarized in Table II. Except for the results of Hillis *et al.*,²⁸ it is seen that pre-equilibrium ef-

fects do not become appreciable until the relative kinetic energy above the Coulomb barrier in the entrance channel is approximately 6–8 MeV/u.

The results for the $^{165}\text{Ho} + ^{56}\text{Fe}$ reaction at 476 MeV can be qualitatively understood by inspecting the relevant time scales for the evaporation time τ_p , nuclear relaxation time τ_R , and interaction time τ_{int} applicable to this experiment as given for different nuclear temperatures in Fig. 12. It appears that for nuclear temperatures reached at a bombarding energy of 4 MeV/u above the Coulomb barrier, even if a hot spot ($T \approx 5 \text{ MeV}$) were formed on contact of the two ions, it would decay within a typical relaxation time τ_R which is short compared to the interaction time ($\tau_R \ll \tau_{\text{int}}$). That is, the system would equilibrate very rapidly to temperatures around 2 MeV where evaporation times are $\approx 10^{-20} \text{ s}$, whereas the corresponding interaction time is of the order $\tau_{\text{int}} \approx 10^{-21} \text{ s}$. Adding to this interaction time the time the two fragments are accelerated within their mutual Coulomb field, one obtains $(5-6) \times 10^{-21} \text{ s}$ which is still smaller than the evaporation time τ_p . From this estimate one expects particles to be evaporated only from the fully accelerated and completely equilibrated fragments.

For incident energies 7–8 MeV/u above the Coulomb barrier, it may be possible to produce local temperatures of 8 MeV if the energy dissipation mechanism would allow an almost instantaneous loss of the available kinetic energy. In this case, the relaxation time τ_R is no longer small compared to the particle-evaporation time τ_p , and one could, indeed, expect a considerable contribution of pre-equilibrium particles.

The essential quantity marking the boundary between the equilibrium and pre-equilibrium regimes appears to be the kinetic energy per nucleon above the Coulomb barrier in the entrance channel rather

TABLE II. Emission of pre-equilibrium neutrons.

Reaction	E_{lab} (MeV)	$(E_{\text{c.m.}} - V_{\text{CB}})/\mu$ (MeV/u)	Measurement		Reference
			a	b	
$^{12}\text{C} + ^{158}\text{Gd}$	152	8.3	CF	+	26
$^{16}\text{O} + ^{154}\text{Sm}$	112–169	2.6–6.3	CF	– to +	27
$^{20}\text{Ne} + ^{150}\text{Nd}$	175	4.6	CF	–	26
$^{56}\text{Fe} + ^{165}\text{Ho}$	476	4.0	SDC/FF	–	Present work
$^{86}\text{Kr} + ^{166}\text{Er}$	602	2.5	SDC	–	24
$^{40}\text{Ar} + ^{124}\text{Sn}$	161–236	0.5–2.4	CF	– to +	28
$^{132}\text{Xe} + ^{197}\text{Au}$	990	2.3	SDC	(+) ^c	29
$^{63}\text{Cu} + ^{197}\text{Au}$	365	0.8	SDC/FF	–	25

^aCF: Complete fusion; FF: Fusion fission; SDC: Strongly damped collisions.

^b+ : evidence; – : no evidence for pre-equilibrium neutrons.

^cSee also Ref. 24. The results of Broek (Ref. 21) are not included since this was an inclusive measurement. He did not observe any pre-equilibrium neutrons though the energies were 8.3–11.8 MeV/u above the Coulomb barrier.

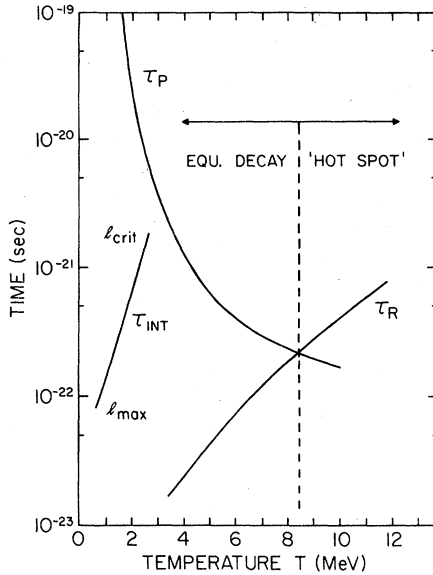


FIG. 12. Relevant time scales in the reaction $^{165}\text{Ho} + ^{56}\text{Fe}$. The curves labeled τ_P , τ_R , and τ_{int} represent the time required to evaporate a particle (Ref. 30) from a nucleus of temperature T , that for the decay of a hot spot in a nucleus of temperature T corresponding to the nuclear relaxation time (Ref. 31), and the nuclear interaction time (Ref. 8) in a nonsticking situation for the given reaction at 476 MeV as a function of equilibrium temperature T , respectively. Only the interaction times that do not lead to fusion ($l > l_{\text{crit}}$) are shown. The smallest interaction time corresponds to the maximum angular momentum (l_{max}).

than the total excitation energy. Using, then, the kinetic energy per nucleon above the Coulomb barrier as a characteristic parameter, one can qualitatively put the (LI, xn) and (HI, xn) reactions on a comparable footing. For both types of reactions pre-equilibrium neutrons are observed for incident energies higher than 5 to 6 MeV/u above the Coulomb barrier³² independent of whether tens or hundreds of MeV of relative kinetic energy have finally been dissipated into intrinsic excitation energy.

This work is supported by the U. S. Department of Energy. It is a pleasure to acknowledge many helpful discussions with Dr. M. Beckerman, who provided us with the evaporation code MBII of Ref. 17. We gratefully acknowledge the help and support of the SuperHILAC staff and user-support organization. The assistance of Dr. M. Zisman was particularly valuable. We are indebted to

Dr. J. C. Davis, Dr. J. C. Brown, Dr. R. N. Boyd, and to the Hahn-Meitner Institut, Berlin, W. Germany, for providing us with neutron detectors and n - γ pulse-shape discrimination units.

APPENDIX

Assuming isotropic emission in the fragment rest frame, the double-differential cross section for neutrons from an evaporation cascade in this frame can be written as¹⁵

$$\frac{d^2\sigma}{d\Omega dE} = \frac{M}{4\pi} \left(\frac{1}{[\Gamma(n+1)] T^{n+1}} \right) E^n \exp(-E/T), \quad (\text{A1})$$

where $\Gamma(n+1)$ is the Γ function, T is an effective nuclear temperature, and M is the neutron multiplicity. The first energy moment $\langle E \rangle$ of this spectrum is given by

$$\langle E \rangle = (n+1)T, \quad (\text{A2})$$

where $\langle E \rangle$ corresponds to the mean kinetic energy carried away per neutron.

If on the average only one particle is evaporated, one has a Maxwellian³³ spectrum with $n=1$ [$\Gamma(2)=1$], whereas for a neutron cascade, LeCouteur and Lang¹⁵ have shown that $n=0.45$. It has experimentally been demonstrated that evaporation spectra of fission neutrons³⁴ can be described very well by using $n=0.5$ [$\Gamma_{\frac{3}{2}} = \sqrt{\pi}/2$], which will be used in the following:

$$\frac{d\sigma^2}{dE_n d\Omega} = \frac{M}{2(\pi T)^{3/2}} \sqrt{E_n} \times \exp[-(E_n - 2\sqrt{\epsilon E_n} \cos\theta + \epsilon)/T], \quad (\text{A3})$$

where E_n is the laboratory neutron energy.

The angular distribution in the lab system is obtained by integrating Eq. (A3) over all neutron energies, yielding

$$\frac{d\sigma}{d\Omega} = \frac{M}{2\pi^{3/2}} \exp\left(\alpha^2 - \frac{\epsilon}{T}\right) \times \left\{ \sqrt{\pi} \left(\alpha^2 + \frac{1}{2}\right) [1 - \text{erf}(c)] + (2\alpha + c) e^{-c^2} \right\}. \quad (\text{A4})$$

The energy spectrum in the lab system is deduced by integrating Eq. (A3) over the angles, yielding

$$\frac{d\sigma}{dE_n} = \frac{M}{2\sqrt{\pi\epsilon T}} \exp\left(\frac{-(E_n + \epsilon)}{T}\right) \sinh\left(\frac{2\sqrt{\epsilon E_n}}{T}\right). \quad (\text{A5})$$

Finally, the dependence of the first moment of the energy spectrum in the lab system on the neutron laboratory angle θ relative to the fragment scattering angle is given by

$$\langle E_n \rangle = \frac{T \left\{ \sqrt{\pi} (3/4 + 3\alpha^2 + \alpha^4) [1 - \text{erf}(c)] + [c^3 + (3/2)c + 4\alpha c^2 + 4\alpha + 6\alpha^2 c + 4\alpha^3] e^{-c^2} \right\}}{\sqrt{\pi} (\alpha^2 + \frac{1}{2}) [1 - \text{erf}(c)] + (2\alpha + c) e^{-c^2}}, \quad (\text{A6})$$

where

$$c = \left(\frac{E_s}{T}\right)^{1/2} - \alpha, \quad \alpha = \left(\frac{\epsilon}{T}\right)^{1/2} \cos\theta,$$

and E_s and ϵ are the neutron energy threshold and the fragment energy/u, respectively.

Particle evaporation leads to a distribution of recoil directions θ of the fragments, which is, however, rather narrow as has been shown by Lide³⁵:

$$\frac{dN(\theta)}{d\Omega} = \frac{2N_0}{2\pi k\chi_k} \cos^2\theta \exp\left(\frac{-\sin^2\theta}{k\chi_k}\right) \quad (\text{A7})$$

and

$$\chi_k = 2 \left(\frac{A\sqrt{mT}}{(A - km)P_i} \right)^2. \quad (\text{A8})$$

Here A is the fragment mass, k is the number of evaporated neutrons, m is the neutron mass, and P_i is the initial fragment momentum. For the reaction $^{165}\text{Ho} + ^{56}\text{Fe}$, this effect leads to a broadening of the fragment angular distribution by only a few degrees.

*On leave of absence from the Hahn-Meitner Institut, Berlin, W. Germany.

¹W. U. Schröder and J. R. Huizenga, *Annu. Rev. Nucl. Sci.* **27**, 465 (1977).

²J. P. Bondorf, in *Proceedings of the European Conference on Nuclear Physics with Heavy Ions*, *J. Phys. C* **5**, 195 (1976); M. C. Robel and W. Swiatecki, private communication.

³D. H. E. Gross and J. Wilczyński, *Phys. Lett.* **67B**, 1 (1977).

⁴J. V. Kratz, H. Ahrens, W. Bögl, W. Brüchle, G. Franz, M. Schädel, I. Warnecke, G. Wirth, G. Klein, and M. Weis, *Phys. Rev. Lett.* **39**, 984 (1977); B. Gatty, D. Guerreau, M. Lefort, X. Tarrago, J. Galin, B. Cauvin, J. Girard, and H. Nifenecker, *Nucl. Phys.* **A253**, 511 (1975).

⁵U. Brosa and H. J. Krappe, *Z. Phys.* **284**, 65 (1978).

⁶A. H. Wapstra and K. Bos, *At. Nucl. Data Tables*, **19**, 177 (1977); **19**, 215 (1977).

⁷Provided and manufactured by the Hahn-Meitner-Institut, Berlin, W. Germany.

⁸A. D. Hoover, J. R. Birkelund, D. Hilscher, W. W. Wilcke, W. U. Schröder, J. R. Huizenga, H. F. Breuer, V. E. Viola, Jr., K. L. Wolf, and A. C. Mignerey, to be published.

⁹R. E. Textor and V. V. Verbinski, ORNL-4160, 1968 (unpublished); and H. Kluge, *Laborbericht*, HMI-P, Berlin, 1971 (unpublished).

¹⁰M. Drog, *Nucl. Instrum. Methods* **105**, 573 (1972).

¹¹K. H. Maier and J. Nitschke, *Nucl. Instrum. Methods* **59**, 227 (1968).

¹²T. G. Masterson, *Nucl. Instrum. Methods* **88**, 61 (1970).

¹³H. R. Bowman, S. G. Thompson, J. C. D. Milton, and W. J. Swiatecki, *Phys. Rev.* **126**, 2120 (1962).

¹⁴W. U. Schröder, J. R. Birkelund, J. R. Huizenga, K. L. Wolf, and V. E. Viola, Jr., *Phys. Rep.* **45C**, 301 (1978).

¹⁵K. L. LeCouteur and D. W. Lang, *Nucl. Phys.* **13**, 32 (1959); D. W. Lang, *ibid.* **53**, 113 (1964).

¹⁶T. Ericson and V. Strutinski, *Nucl. Phys.* **8**, 284 (1958); T. Ericson, *Adv. Phys.* **9**, 425 (1960).

¹⁷M. Beckerman and M. Blann, University of Rochester Report UR-NSRL-135 (1977).

¹⁸M. M. Aleonard, G. J. Wozniak, P. Glässel, M. A. Deleplanque, R. M. Diamond, L. G. Moretto, R. P.

Schmitt, and F. S. Stephens, *Phys. Rev. Lett.* **40**, 622 (1978).

¹⁹A. Olmi, H. Sann, D. Pelte, Y. Eyal, A. Gobbi, W. Kohl, U. Lynen, G. Rudolf, H. Stelzer, and R. Bock, *Phys. Rev. Lett.* **41**, 688 (1978).

²⁰G. Wolschin and W. Norenberg, *Phys. Rev. Lett.* **41**, 691 (1978).

²¹H. W. Broek, *Phys. Rev.* **124**, 233 (1961).

²²W. D. Myers and J. Swiatecki, *Ann. Phys. (N. Y.)* **55**, 395 (1969).

²³F. Plasil, R. L. Ferguson, H. C. Britt, R. H. Stokes, B. H. Erkkila, P. D. Goldstone, M. Blann, and H. H. Gutbrod, *Phys. Rev. Lett.* **40**, 1164 (1978).

²⁴Y. Eyal, A. Gavron, I. Tserruya, Z. Fraenkel, Y. Eisen, S. Wald, R. Bass, G. R. Gould, G. Kreyling, R. Renfordt, K. Stelzer, R. Zitzmann, A. Gobbi, U. Lynen, H. Stelzer, I. Rode, and R. Bock, *Phys. Rev. Lett.* **41**, 625 (1978).

²⁵J. Péter, M. Berlinger, C. Ngo, B. Tamain, B. Lucas, C. Mazur, M. Ribrag, and C. Signarbieux, *Z. Phys.* **A283**, 413 (1977).

²⁶L. Westerberg, D. G. Sarantites, D. C. Hensley, R. A. Dayras, M. L. Halbert, and J. H. Barker, *Phys. Rev. C* **18**, 796 (1978).

²⁷K. A. Geoffroy, D. G. Sarantites, L. Westerberg, J. H. Barker, D. C. Hensley, R. A. Dayras, and M. L. Halbert, *Bull. Am. Phys. Soc.* **23**, 950 (1978).

²⁸D. L. Hillis, O. Christensen, B. Fernandez, A. J. Ferguson, J. D. Garrett, G. B. Hagemann, B. Herskind, B. B. Back, and F. Folkmann, *Phys. Lett.* **78B**, 405 (1978). The results of Hillis *et al.* are somewhat difficult to apply to the problem under consideration. These authors deduced the mean energy $\langle E_n \rangle$ carried away per neutron as a function of the number of neutrons emitted from the completely fused system by measuring the mean γ -ray multiplicity and energy. At 2.4 MeV/u (see Table II) above the Coulomb barrier they deduce mean neutron energies $\langle E_n \rangle$ above and below the expected thermal value for the (HI, 6n) and (HI, 9n) events. However, by selecting only the 6n and 9n channels, one samples predominantly the high- and low-energy ends of an evaporation spectrum, respectively. Hence, it is not permissible to use only the mean neutron energies from the (HI, 6n) reaction as an indication for non-thermal, preequilibrium events. If one measures simultaneously, however, also the neutron energy spec-

- tra, as has been done by Westerberg *et al.* (Ref. 26), this method can be a powerful tool to look specifically at pre-equilibrium neutrons. A conclusion similar to that above has been reported recently by M. Blann and R. L. Ferguson, *Phys. Rev. C* 19, 298 (1979).
- ²⁹C. R. Gould, R. Bass, J. V. Czarnecki, V. Hartmann, K. Stelzer, R. Zitzmann, and Y. Eyal, *Z. Phys.* A284, 353 (1978).
- ³⁰R. G. Stokstad, in *Proceedings of the Topical Conference on Heavy-Ion Collisions*, Falls Creek Falls State Park, Tennessee (U. S. Department of Commerce, 1977).
- ³¹A. Kind and Patergnani, *Nuovo Cimento* 10, 1375 (1953).
- ³²We wish to emphasize that the comparison of heavy ion and light ion data based on the characteristic parameter bombarding energy/u above the Coulomb barrier is only approximate. However, this parametrization is much superior to a comparison based on the total excitation energy. As an example, pre-equilibrium particle emission is only a few percent of the reaction cross section for ^3He induced reactions on targets of $A \approx 60$ at an incident energy of 25.6 MeV, which is about 5 MeV/u above the Coulomb barrier. [S. Chevarier *et al.*, *Nucl. Phys.* A231, 64 (1974)]. At a higher incident energy of 42 MeV for the $^{58}\text{Ni}(\alpha, p)$ reaction, corresponding to 7–8 MeV/u, pre-equilibrium protons make up about 6% of the total yield of emitted protons [R. W. West, *Phys. Rev.* 141, 1033 (1966)]. This latter reaction is a good case for comparison purposes because essentially the entire reaction cross section goes into proton emission.
- ³³V. Weisskopf, *Phys. Rev.* 52, 295 (1937).
- ³⁴B. E. Watt, *Phys. Rev.* 87, 1037 (1952).
- ³⁵R. W. Lide, ORNL-Report-3358 (1967).